RESEARCH PAPER

A simple estimation model for basal heave stability of braced excavations in anisotropic clay

Runhong Zhang[1,2] · Anthony Teck Chee Goh[5] · Yongqin Li[3] · Hanlong Liu[3,4] · Lin Wang[3] ·
Zhixiong Chen[3] · Wengang Zhang[3,4] 🔟

Abstract

The basal heave stability of the excavation and support system is a major concern to geotechnical design engineers, particularly in soft clay deposits. Conventional methods for estimating the basal heave stability of braced excavations generally do not consider the anisotropy of the soft clay, which may lead to the incorrect assessment of excavation stability. This study presents the results of extensive finite element analysis to investigate the influence of clay anisotropy on basal heave stability. The parameters that were considered include the ratio of the plane strain passive shear strength to the plane strain active shear strength s_u^P/s_u^A, the ratio of the unloading/reloading shear modulus to the plane strain active shear strength G_{ur}/s_u^A, the plane strain active shear strength s_u^A, soil unit weight γ, wall system stiffness $\ln(S)$, excavation width B, excavation depth H_e, and the wall penetration depth D. A simple logarithmic regression model was developed for preliminary assessment of the basal heave factor of safety for braced excavations in anisotropic clay. Validations from case histories indicate that the proposed model can provide reasonable predictions of the basal heave stability in soft clay.

Keywords Anisotropy · Basal heave · Braced excavation · Case validations · Estimation model

1 Introduction

It has generally been recognized that the behavior of many clays is anisotropic. This behavior has been explicitly accounted for in many geotechnical analyses including slope stability [5, 27], and embankment stability [4, 38]. However, not as much attention has been devoted to assessing the effects of clay anisotropy on the response of

✉ Wengang Zhang
zhangwg@cqu.edu.cn

1 Institute for Smart City of Chongqing University in Liyang, Chongqing University, Liyang 213300, Jiangsu, China

2 College of Aerospace Engineering, Chongqing University, Chongqing 400045, China

3 School of Civil Engineering, Chongqing University, Chongqing 400045, China

4 Key Laboratory of New Technology for Construction of Cities in Mountain Area, Chongqing University, Chongqing 400045, China

5 School of Civil and Environmental Engineering, Nanyang Technological University, Singapore 639798, Singapore

braced excavation. Most conventional methods for estimating the basal heave stability of braced excavations use the limit equilibrium approach and generally assume that the strength of the soil is isotropic. Examples of such methods include Terzaghi [28], Bjerrum and Eide [2], Goh [9], Hsieh et al. [14], Goh et al. [10], Tang and Kung [26], Wu et al. [32], Luo et al. [22], Chowdhury [3], Wu et al. [34], Goh [11], Goh et al. [12], Wu et al. [33], Zhang et al. [39], Lyn et al. [23] and Zhang et al. [40]. According to Shen [24], Huang and Liu [15], Ying et al. [35], Li and Zhang [21], soft clays in coastal cities of China, such as Shanghai, Hangzhou, and Tianjin, are generally inherently anisotropic in both strength and stiffness, which implies that the strength and stiffness have different magnitudes depending on the orientation of the major principal stress (α) when the soil is sheared, as shown schematically in Fig. 1.

The anisotropic behavior of soft clay has been investigated by many researchers. Hanson and Clough [13] investigated the influence of anisotropy of soft to medium clays on basal heave potential, wall and soil movements, and earth pressures using the finite element method and
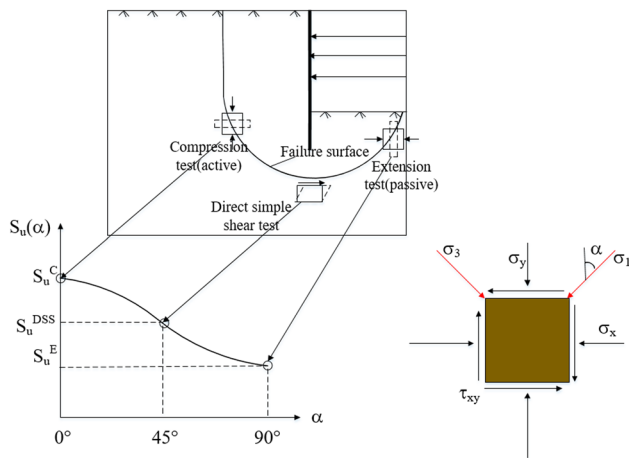
Fig. 1 Anisotropic undrained shear strength according to the orientation of principal stresses (after [8])

concluded that anisotropy resulted in a decrease of the basal heave factor of safety, increase of ground and wall movements and alteration of the earth pressure distribution acting on the wall. Subsequently, they proposed that the effect of anisotropy can be approximately included in isotopic analyses by using an estimate of the shear strength which is lower than the conventional compressive strength. Wheeler et al. [31] developed an anisotropic elastoplastic model for Otaniemi clay from Finland and found it outperforms the Modified Cam Clay model. Kong et al. [18] adopted the Casagrande anisotropy strength theory and limit equilibrium method and derived a formulation for the basal heave stability for deep excavations in anisotropic soft clays. Teng et al. [29] conducted a series of tests on tube samples in anisotropic Taipei soft clay and concluded that the anisotropy ratio for the shear modulus ranged between 1.15 and 1.44. They also proposed that the anisotropy ratio for Young's modulus ranged between 1.38 and 1.54 at a strain of 0.00001. D'Ignazio et al. [4] conducted a finite element analysis by adopting the NGI-ADP Soft (anisotropic total stress constitutive model) [7] to back-analyze a full-scale test with data collected from the experiment and laboratory test. Ismae et al. [16] proposed and validated a new constitutive model called 'Transubi model' for Opalinus clay that possesses anisotropy in strength and stiffness and shows non-linear behavior in the pre-and post-yield regions. Zhang et al. [41, 42] carried out extensive finite-element analyses to examine the responses of braced excavation in anisotropic clay using the total stress-based anisotropic model NGI-ADP [8]. However, the effects of the anisotropic characteristics of clay on the basal heave of braced excavations were not systematically investigated. To be specific, currently, no empirical or semi-empirical model has been proposed that relates the factor of safety against basal heave for braced excavations

in anisotropic clay to the various parameters such as the strength and stiffness anisotropy ratios, etc.

The focus of this paper is on the assessment of basal heave instability for deep excavations in anisotropic clay. The total stress-based anisotropic model NGI-ADP [8] was employed to model the behavior of the soft clay. Extensive finite element (FE) analyses were carried out to assess the basal heave factor of safety for braced excavations. The effects of several soil and wall parameters on basal heave factor of safety were systematically investigated, including the ratio of the plane strain passive shear strength to the plane strain active shear strength s_u^P/s_u^A, the ratio of the unloading/reloading shear modulus to the plane strain active shear strength G_{ur}/s_u^A, the plane strain active shear strength s_u^A, soil unit weight γ, wall system stiffness $\ln(S)$, excavation width B, excavation depth H_e, and the wall penetration depth D. Based on the extensive numerical analyses, a simplified estimation model is proposed for preliminary assessment of the basal heave factor of safety for braced excavations in anisotropic clay.

2 Soil model

The NGI-ADP model [8] is an anisotropic shear strength model for clay in which the undrained shear strength s_u profiles for active (A), direct simple shear (DSS), and passive (P) loading (stress paths) are given as input data. The model interpolates anisotropic undrained shear strength between s_u^C, s_u^{DSS}, and s_u^E along the failure surface according to the orientation of principal stresses as defined in Fig. 1.

The main soil parameters of the NGI-ADP model are G_{ur}/s_u^A (ratio of the unloading/reloading shear modulus to the plane strain active shear strength), γ_f^C (shear strain at failure under triaxial compression), γ_f^E (shear strain at failure under triaxial extension), and γ_f^{DSS} (shear strain at failure under direct simple shear). The soil strength includes $s_{u,ref}^A$ (reference plane strain active shear strength), $s_u^{C,TX}/s_u^A$ (ratio of the triaxial compressive shear strength to the plane strain active shear strength), y_{ref} (reference depth), $s_{u,inc}$ (increase in the shear strength with increasing depth), s_u^P/s_u^A (ratio of the plane strain passive shear strength to the plane strain active shear strength), τ_0/s_u^A (initial mobilization), s_u^{DSS}/s_u^A (ratio of the direct simple shear strength to the plane strain active shear strength) and Poisson's ratio υ_u. $s_{u,ref}^A$ represents the shear strength obtained in (plane strain) undrained active stress paths for the reference depth y_{ref}. Additional details are referred to in Brinkgreve et al. [1].

3 Finite element modeling

3.1 Case study

This section introduces an excavation case of metro station in Hangzhou city, China. The stratigraphy of Hangzhou city contains soft clay that shows stress anisotropic behavior. The width and length of the excavation are approximately 20 m and 291 m as shown in Fig. 2, and the final excavation depth is 17.0 m. The buildings near the excavation area are high-rise buildings (height = 60–120 m) and podium building (height = 18 ~ 24 m) supported by pile foundation. In this section, the plane strain finite element analysis for the excavation was carried out by software PLAXIS2D [1], and the finite element results are validated by the instrument monitoring data.

The excavation system consisted of 34.8 m long diaphragm walls and five levels of struts, installed at − 2 m, 6.1 m, 9.9 m, 11.4 m, and 12.9 m, respectively. The groundwater table is at a depth of − 2.5 m. The soil was modeled by 15-noded triangular elements, the undrained total stress of the soft soil was adopted in the analysis. The diaphragm wall was assumed to be linearly elastic and modeled by 5-noded beam elements, the struts were modeled by 3-noded bar elements, and the interface between the wall and the soil were assumed as rigid (R_{inter} = 1.0). The side boundaries were fixed on the horizontal displacement, and the bottom boundary was constrained both horizontally and vertically. The right vertical boundary has been extended far enough from the excavation area to eliminate the boundary effects. A typical finite element mesh is shown in Fig. 3.
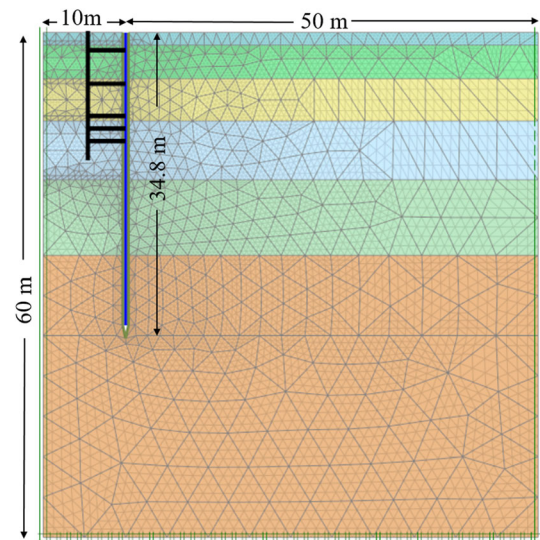

Fig. 3 The geometry and typical mesh of the FE model

According to Larsson [19], and Larsson et al. [20], the empirical equations of s_u^A/σ_v', s_u^{DSS}/σ_v', s_u^P/σ_v' are as follows:

$$\frac{s_u^A}{\sigma_v'} = 0.33 \text{OCR}^{0.8} \tag{1}$$

$$\frac{s_u^{DSS}}{\sigma_v'} = \left(0.125 + 0.205 \frac{w_L}{1.17}\right)\text{OCR}^{0.8} \tag{2}$$

$$\frac{s_u^P}{\sigma_v'} = \left(0.055 + 0.275 \frac{w_L}{1.17}\right)\text{OCR}^{0.8} \tag{3}$$

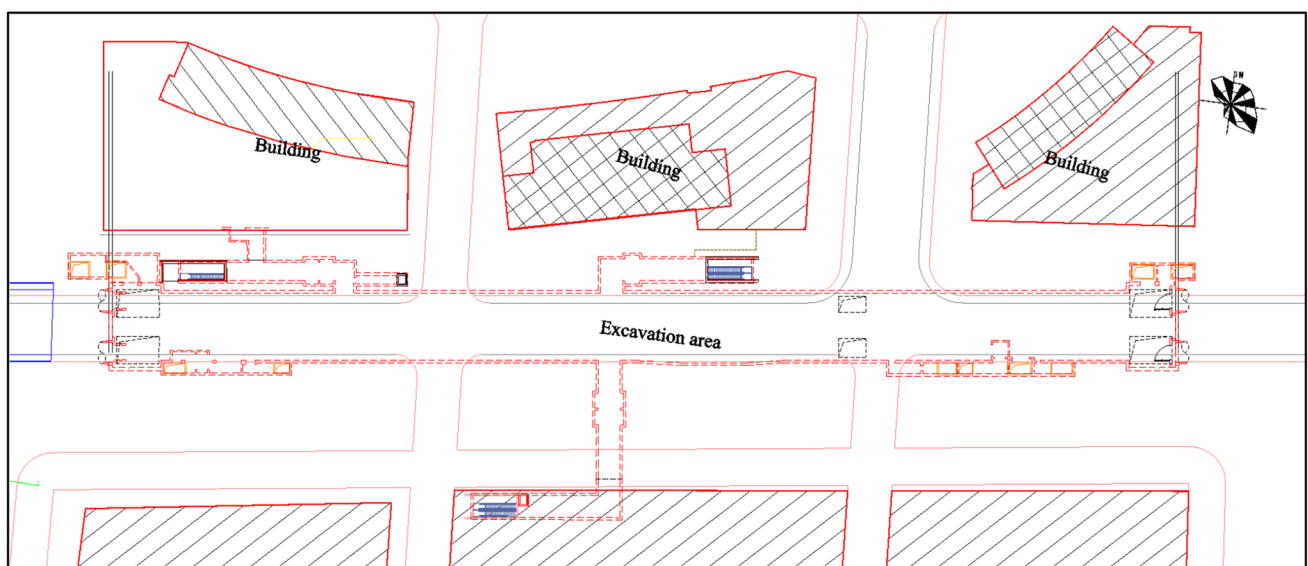In this study, the s_u^{DSS}/s_u^A, s_u^P/s_u^A can be obtained by:

Fig. 2 Plan view of the excavation area (scale 1:1000)

$$\frac{s_u^{DSS}}{s_u^A} = \frac{\left(0.125 + 0.205 \frac{w_L}{1.17}\right)}{0.33} \tag{4}$$

$$\frac{s_u^P}{s_u^A} = \frac{\left(0.055 + 0.275 \frac{w_L}{1.17}\right)}{0.33} \tag{5}$$

The soil parameters of the site are listed in Table 1.

As shown in Fig. 4, the FE calculated maximum wall deflection is consistent with the measured inclinometer data, as well as the location of the deflection point. The shape of the curve is a bit different in that the top half for the measured deviates from the regular pattern possibly due to the influences from the adjacent buildings. The NGI-ADP model has been analyzed and adopted in FEM by many researchers. Fu et al. [6] found that the expression adopted by the NGI-ADP model is demonstrated to be capable of describing the stress–strain response of different clays under undrained conditions. Yz and Kha [37] demonstrated that the NGI-ADP model is capable of describing the stress–strain responses measured over a wide range of natural clays. Skau et al. [25] used NGI-ADP model for modeling the soil of a three-dimensional FE model with a foundation, and the accuracy of the FEA was assessed by comparing computed normalized failure envelopes. The FE model that employed NGI-ADP soil constitutive model in this study is reliable and can be used for further parametric sensitivity analysis.

3.2 Simplified model for parametric study

This section describes the simplified soil profile that was used for the total stress plane strain parametric study to analyze the braced excavation performance in anisotropic clay. The FE model comprises of supporting structures including retaining wall and four levels of struts, and 40 m deep soft clay layer overlying a 20 m stiff clay layer. Figure 5 shows the schematic cross-section of the excavation system. The struts were located at depths of 1 m, 3 m, 5 m, and 7 m below the original ground surface. The NGI-ADP constitutive model was used for the soft clay
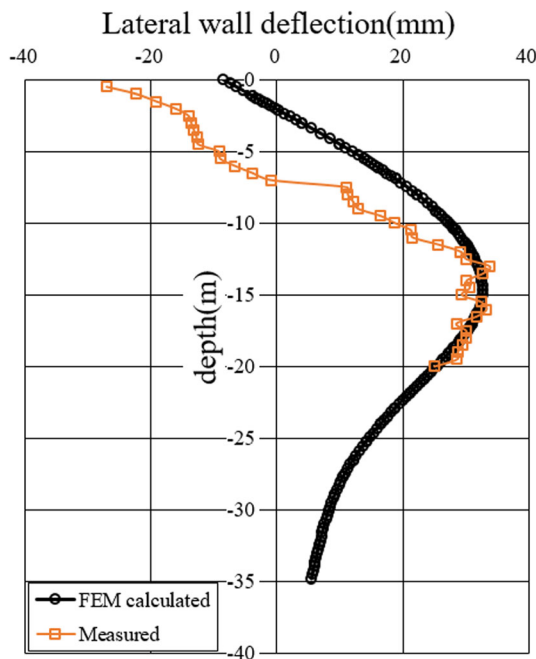

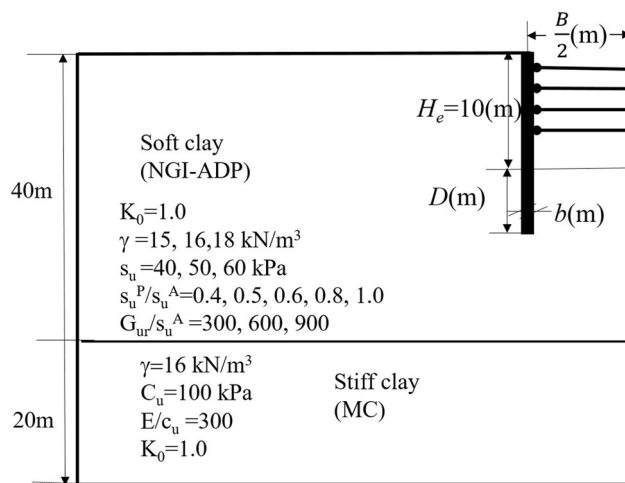**Fig. 4** Comparison between FEM calculated and measured wall deflection

Fig. 5 The cross-sectional profile of the simplified FE model

Table 1 Soil properties of the excavation in Hangzhou city

Soil type	Depth (m)	γ (kN/m³)	E (kPa)	e (−)	K_0 (−)	G_{ur}/s_u^A (−)	$s_{u,ref}^A$ (kPa)	$s_{u,inc}^A$ (kPa)	s_u^P/s_u^A (−)	s_u^{DSS}/s_u^A (−)
Fill	− 1.5	19.0	8000	0.6	0.6	300	20	0	1	1
Clay	− 5.5	19.8	7470	0.767	0.45	300	2.72	2.48z*	0.45	0.59
Silt clay 1	− 10.5	19.2	6020	0.851	0.55	300	16.35	2.61z	0.41	0.56
Silt clay 2	− 17.5	19.0	5420	0.898	0.5	600	43.75	3.64z	0.41	0.56
Silt clay3	− 26.5	18.8	4980	0.923	0.6	900	107.46	2.64z	0.41	0.56
Silt clay4	− 36.0	19.2	12,460	0.822	0.4	900	177.33	3.17z	0.36	0.52

*z is the depth of the soil below the ground surface

[30] while the Mohr–Coulomb (Undrained C) model was used for modeling the stiff clay. The excavation width B, the wall system stiffness $\ln(S)$, the final excavation depth H_e, and the penetration depth of the wall below the formation level D are shown schematically in Fig. 5. The strut stiffness per meter EA is 6.1×10^5 kN/m. For simplicity, the elastic modulus of the wall E_{wall} is assumed to be constant and equal to 2.8×10^7 kPa, and the rigidity (stiffness) of the wall is studied by varying the wall width b. The ranges of three critical soil parameters considered in this study including s_u^A (kPa), $G_{ur}/s_u^A(-)$, and $s_u^P/s_u^A(-)$ are also shown in Fig. 5. The range of s_u^P/s_u^A considered in this study is 0.4, 0.5, 0.6, 0.8, and 1.0, with $s_u^P/s_u^A = 1.0$ denoting that the clay is isotropic, and a smaller value of s_u^P/s_u^A indicating a higher degree of strength anisotropy of the clay.

From symmetry, only half of the cross-section is considered as shown in Fig. 5. The right vertical boundary extends 60 m from the excavation edge to minimize the effects of the boundary restraints. The nodes along the left and right boundaries were constrained horizontally and the bottom boundary was constrained both vertically and horizontally. The soil was modeled using 15-noded triangular elements, the structural elements of the wall were assumed to be linearly elastic and modeled by 5-noded beam elements, and the struts were represented by 3-noded bar elements.

The parametric study was carried out with an emphasis on the basal heave factor of safety for braced excavation in anisotropic clay, using the NGI-ADP model for the soft clay layer. The stability of the excavation was then determined using the shear strength reduction technique as detailed in Brinkgreve et al. [1]. The properties of the soft and stiff clay are listed in Table 2. This study based on the recommendations of Brinkgreve et al. [1]. the $s_u^{C,TX}/s_u^A$ and τ_0/s_u^A ratios are set to their default values of 0.99 and 0.7, respectively. The structural properties of the support system are shown in Table 3. A total of 2523 different finite element analyses were carried out in this study.

3.3 Batch finite element modeling

The parametric finite element study was very challenging because of the number of different parameters that were varied. To enhance the efficiency and accuracy of the input data process and evaluating the output data, an efficient procedure for automating the FEM is developed in this study, as shown in Fig. 6. The pre-processing and post-processing of the FEM are realized through the macro function in EXCEL and the codes in Python, respectively, and the calculation is carried out through a batch file command. The specific procedures are shown in Fig. 6.

1. Establish a sample model in PLAXIS2D, which is a simplified two-dimensional finite element model.
2. Generate commands to change soil parameters in EXCEL.
3. Input the generated command into PLAXIS, run and generate finite element models with different soil parameters.
4. Create and run a BATCH file to start the PLAXIS calculation program.
5. Open the pre-generated finite element models one by one, mesh each model, run calculations, and save them independently, until all models are calculated.
6. Use Pycharm to connect to PLAXIS' Python compiler and use pre-written code (attached in appendix) to output the results of the calculated model, including the maximum lateral displacement of the retaining wall, the safety factor of the basal heave, and the axial force of each strut.
7. Sort out and analyze the data that has been exported to EXCEL.

4 Results and analyses

Some typical soil displacement contours for the anisotropic and isotropic cases are shown in Fig. 7. For isotropic cases, the maximum soil displacement occurs at the center of formation level. The influence of the s_u^P/s_u^A on the soil

Table 2 Soil model properties

Soft clay (NGI-ADP)	Parameter	$s_u^{C,TX}/s_u^A(-)$	$\gamma_f^C(\%)$	$\gamma_f^{DSS}(\%)$	$\gamma_f^E(\%)$	$\upsilon_u(-)$	$s_u^{DSS}/s_u^A(-)$	
	Value	0.99	0.75	1.735	3.5	0.495	$(1 + s_u^P/s_u^A)/2$	
	Parameter	$\tau_0/s_u^A(-)$	$R_{inter}(-)$	s_u^A (kPa)	γ (kN/m³)	$G_{ur}/s_u^A(-)$	$s_u^P/s_u^A(-)$	
	Value	0.7	1	40, 50, 60	15, 16, 18	300, 600, 900	0.4, 0.5, 0.6, 0.8, 1.0	
Stiff clay (MC)	Parameter	γ (kN/m³)	c_u (kPa)	$K_o = 1 - \sin\phi$ (−)	ϕ_u (°)	E/c_u (−)	υ_u (−)	R_{inter} (−)
	Value	16	100	1	0	300	0.495	1

Table 3 Parameters of the excavation supporting system and geometry

Parameter and units	Ranges
Horizontal strut spacing $L_{spacing}$ (m)	4
Average vertical strut spacing h_{avg} (m)	2
Strut stiffness per meter EA (kN/m)	6.1×10^5
Elastic modulus of wall E_{wall} (kPa)	2.8×10^7
System stiffness ratio ln(S)* (-)	3.90, 4.76, 5.43, 8.06, 8.92, 10.13
Excavation width B (m)	20, 30
Final excavation depth H_e (m)	10, 16
Wall penetration depth D (m)	3, 5, 10

*In which $S = (EI)_{wall}/\gamma_w h_{avg}^4$, where $(EI)_{wall}$ is the wall stiffness, γ_w is the unit weight of water and h_{avg} is the average vertical strut spacing

displacement is significant, with the maximum soil displacement for $s_u^P/s_u^A = 0.5$ approximately 175% larger than the maximum soil displacement for $s_u^P/s_u^A = 1.0$.

Figure 8 shows the comparison of the basal heave factor of safety FS for some typical anisotropic and isotropic cases. It indicates that a larger s_u^P/s_u^A ratio results in a lower FS for the anisotropic soil. It also shows that the wall system stiffness ln(S) has considerable influence on the FS only when the magnitude of ln(S) is small, i.e., flexible wall; while for the stiff walls, the ln(S) shows a marginal influence on the FS. In addition, ln(S) shows a larger effect on the FS when the soil is anisotropic compared with the isotropic case.

Figure 9 shows the influence of s_u^A and s_u^P/s_u^A on the FS. The FS increases almost linearly as s_u^P/s_u^A increases, which indicates that the soil anisotropy has a significant influence on the stability of the basal heave. As expected, the FS increases as the s_u^A increase, the active undrained shear strength has a positive effect on the basal heave stability. The plot also indicates that the relationship between the FS and s_u^A is also nearly linear as inferred by the approximately equal intervals between the lines.

Figures 10 and 11 show the influence of the D/H_e and G_{ur}/s_u^A on the FS, respectively. The D/H_e and G_{ur}/s_u^A both show marginal influence on the FS. Considering that the thickness of the soft clay is greater than the wall penetration depth, and the fact that the wall was not inserted into
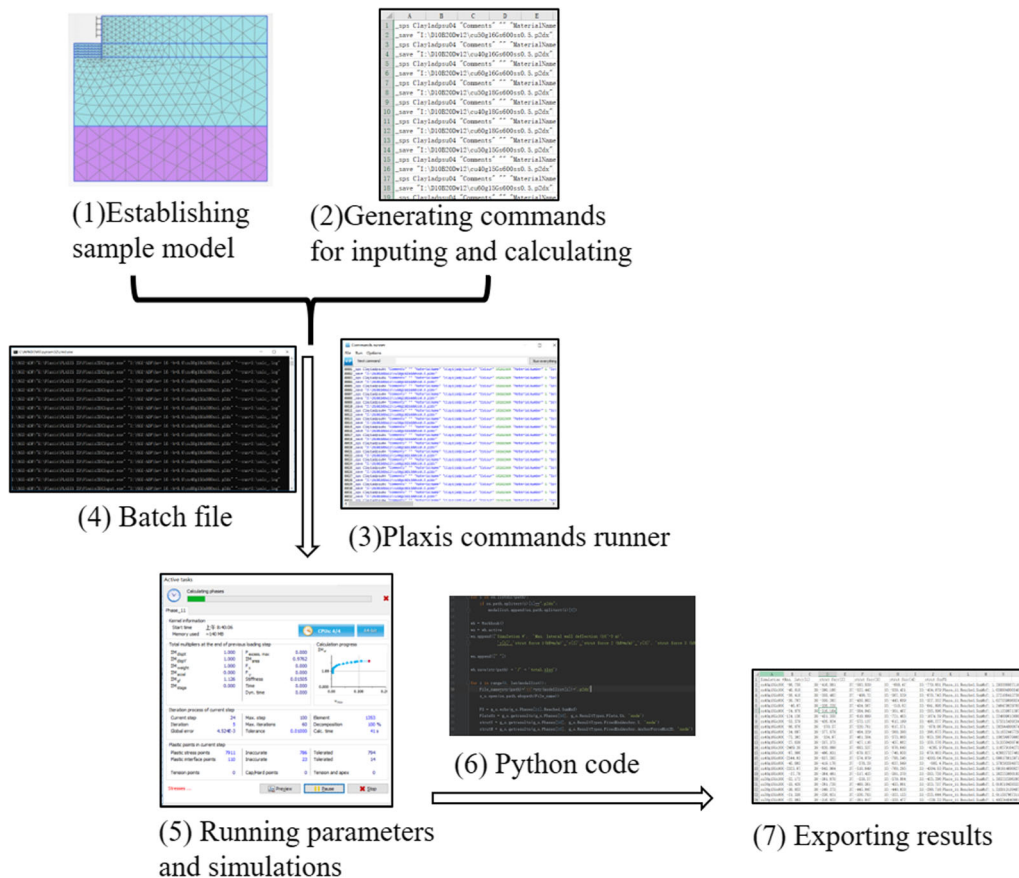

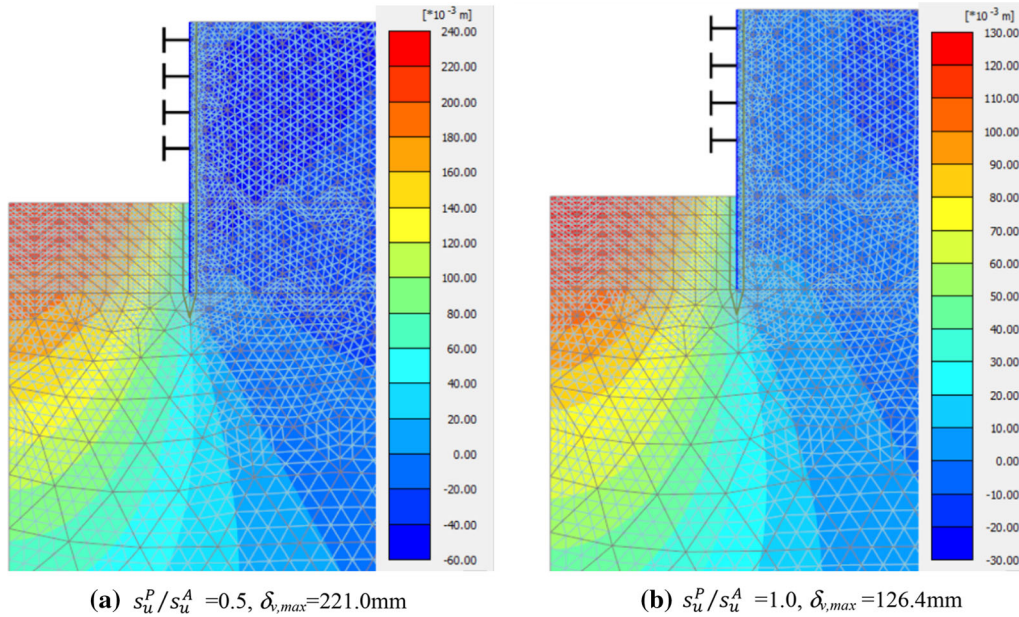**Fig. 6** Flow chart for batch FE modeling of braced excavations in anisotropic clay

(1) Establishing sample model

(2) Generating commands for inputing and calculating

(4) Batch file

(3) Plaxis commands runner

(5) Running parameters and simulations

(6) Python code

(7) Exporting results

(a) s_u^P/s_u^A =0.5, $\delta_{v,max}$=221.0mm

(b) s_u^P/s_u^A =1.0, $\delta_{v,max}$ =126.4mm

Fig. 7 Comparison of typical soil displacement contours for anisotropic and isotropic cases (B/H_e = 2, D/H_e = 0.5, γ = 16 kN/m³, s_u^A = 40 kPa, G_{ur}/s_u^A = 600, ln(S) = 8.92)
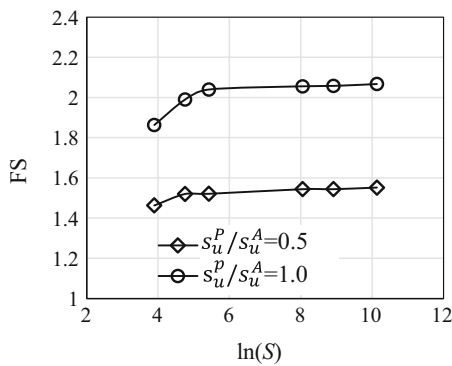

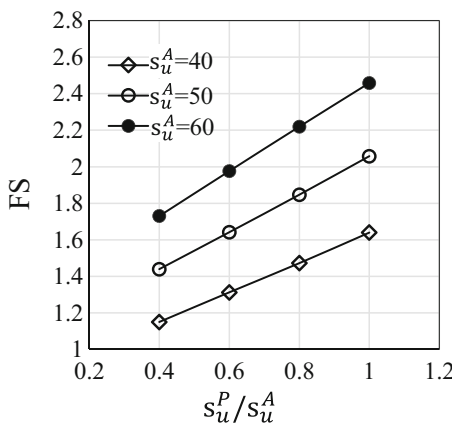**Fig. 8** Comparison of FS for anisotropic and isotropic cases (B/H_e = 2, D/H_e = 0.5, γ = 15 kN/m³, s_u^A = 50 kPa, G_{ur}/s_u^A = 600.)

the hard stratum, D/H_e produces little influence on the basal heave, especially when D/H_e is between 0.5 and 1.0.

Figure 12 which shows the effect of the soil unit weight γ on the FS. Soil unit weight is proven to be important factor for the basal heave, and most of the empirical equations of FS include γ. The empirical equations proposed by Goh et al.[12] indicates that there are inverse proportional relationship between the FS and the γ, and it can be observed in Fig. 12 that the FS decreases almost linearly with the increase of γ.
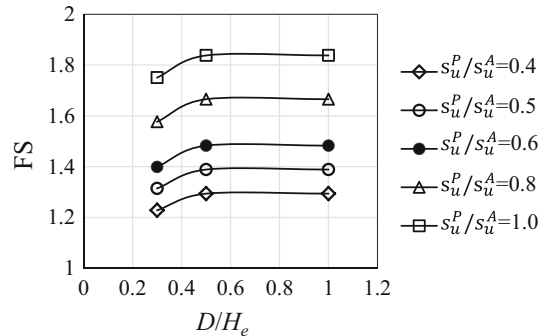

Fig. 9 Influence of s_u^A and s_u^P/s_u^A on the FS (B/H_e = 2, D/H_e = 0.5, γ = 16 kN/m³, ln(S) = 8.92, G_{ur}/s_u^A = 600)

Fig. 10 Influence of D and s_u^P/s_u^A on the FS (B/H_e = 2, γ = 16 kN/m³, ln(S) = 8.06, s_u^A = 50 kPa, G_{ur}/s_u^A = 600)
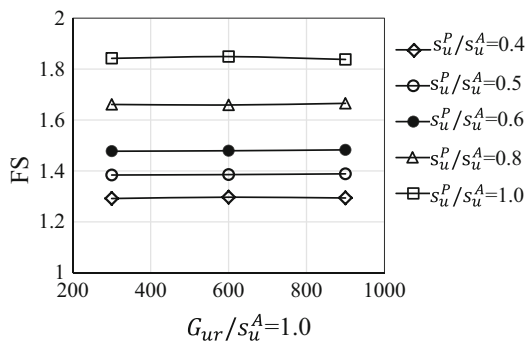
Fig. 11 Influence of G_{ur}/s_u^A and s_u^P/s_u^A on the FS (B/H_e = 2, D/H_e = 0.5, γ = 18 kN/m³, $\ln(S)$ = 8.06, s_u^A = 50 kPa)

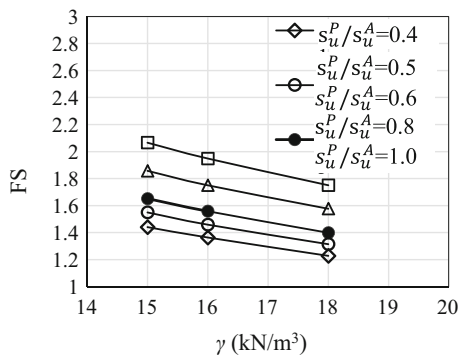**Fig. 12** Influence of γ and s_u^P/s_u^A on the FS (B/H_e = 2, D/H_e = 0.5, $\ln(S)$ = 8.06, s_u^A = 50 kPa, G_{ur}/s_u^A = 900)

5 Estimation models of FS

Based on the numerical results of a total of 2523 hypothetical cases, the logarithmic regression (LR) model is used to develop a simple predictive model to determine the FS against basal heave for braced excavations in anisotropic clay, with coefficient of determination of R^2 = 0.8751, The logarithmic regression FS equation is as follows:

$$FS\_LR = 0.506(D/H_e)^{0.0601}(B/H_e)^{0.2157}\ln(S)^{0.0374}$$
$$(s_u^A)^{0.9289}\gamma^{(-0.8652)}(G_{ur}/s_u^A)^{(-0.0197)}(s_u^P/s_u^A)^{0.3596}$$

The comparison of the factor of safety computed by the finite element analysis FS_FEM and FS_LR is shown in Fig. 13.

The parameter sensitivity is also evaluated and the results are shown in Fig. 14. The sensitivity index (SI) was used to assess the relative importance of each variable. The SI is calculated by changing one variable at a time over ± 10% from the mean and determining the percent change in the FS. This simple indicator provides a good indication of parameter and model variability. The results
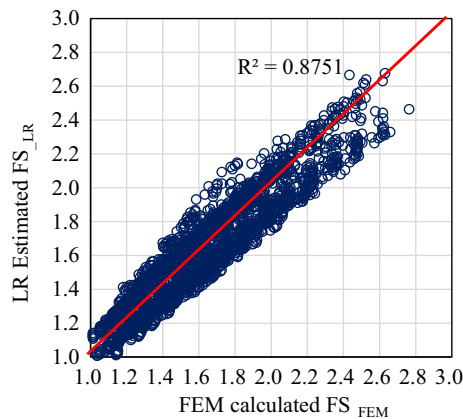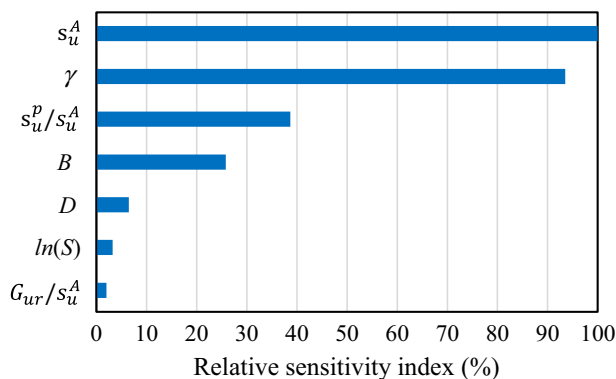

Fig. 13 Comparison of FS_FEM and FS_LR

Fig. 14 Parameter sensitivity

indicate that the influence of the parameters s_u^A, γ, s_u^P/s_u^A, and B/H_e on the FS are more significant compared with the parameters D/H_e, $\ln(S)$, and G_{ur}/s_u^A.

6 Model validation

This section presents the validation of the proposed LR model based on 10 Hangzhou case histories from Ying et al. [36] and 3 Taiwan cases from Hsieh et al. [14]. For Hangzhou case, the depths of the excavations were in a range of 9.5–14.9 m and wall depths ranges from 19.5 to 35 m. The ratios of embedded depths to excavation depths varied from 0.91 to 1.46. The undrained shear strength obtained from field vane shear tests varies from 25 to 40 kPa, the average total unit weight of the clays is about 17 kN/m³. The support walls comprised of contiguous piles with diameters and spacing that ranged from 0.8 to 1.0 m and from 1.0 to1.40 m, respectively. The parameters of the case histories adopted in this study are listed in Table 4. The basal heave factor of safety FS_S2 is obtained by the simplified method S2 proposed by Hsieh et al. [14]. In the S2 method, the undrained shear strength $(s_u)_{avg}$ is derived

Table 4 The documented case of excavations in soft clay

No.	D/H_e (−)	B/H_e (−)	$\ln(S)$ (−)	s_u^A (kPa)	γ (kN/m³)	G_{ur}/s_u^A(−)	s_u^P/s_u^A(−)	FS_LR	FS_S2	References
1	0.91	13.82	7.43	25	17	600	0.4	1.04	0.85	Ying et al. [36]
2	1.43	4.05	6.03	25	17	600	0.4	0.81	0.71	
3	1.04	4.85	5.59	35	17	600	0.4	1.13	1.20	
4	1.10	6.25	5.42	35	17	600	0.4	1.20	1.29	
5	1.21	4.64	6.15	35	17	600	0.4	1.14	1.20	
6	1.34	10.53	5.67	25	17	600	0.4	0.99	0.86	
7	1.19	3.13	5.67	25	17	600	0.4	0.76	0.89	
8	1.35	8.05	5.92	30	17	600	0.4	1.11	0.63	
9	1.16	12.40	5.84	25	17	600	0.4	1.02	0.65	
10	1.46	4.39	6.43	35	17	600	0.4	1.14	0.81	
11	0.78	1.93	6.89	40	18	600	0.61	1.15	1.00	Hsieh et al. [14]
12	0.66	1.32	7.5	35	18	600	0.56	0.90	0.88	
13	0.83	1.32	7.5	35	18	600	0.56	0.92	0.99	

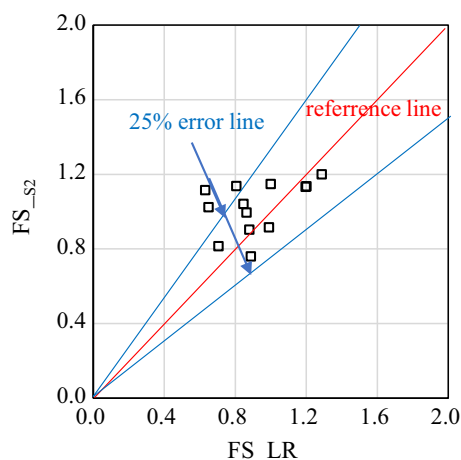from the average value of the CK0U-AC and CK0U-AE test results:

$$(s_u)_{avg} = \frac{s_u^e + s_u^c}{2} = \frac{s_u^P + s_u^A}{2}$$

And the FS_S2 are calculated by the slip circle method:

$$\text{FS}_{S2} = \frac{M_r}{M_d} = \frac{X' \int_0^{\frac{\pi}{2}+\rho} s_u(X' d\theta)}{W \frac{X'}{2}}$$

where s_u is the undrained shear strength of clay; X' is the radius of the failure arc; W is the total weight of the soil and surcharge above the excavation surface within an X' wide area outside the retaining construction; θ is the angle between the failure surface and the vertical direction, and ρ is the angle of failure arc in the excavation zone.

Figure 15 and Table 4 present the comparison between FS_S2 and FS_LR for 10 Hangzhou and 3 Taiwan cases, the

Pearson correlation coefficient of the FS_S2 and FS_LR is 0.43, indicate a good agreement between the two methods.

7 Summary and conclusions

In this paper, extensive FE analysis has been carried out to analyze the effects of the s_u^P/s_u^A, G_{ur}/s_u^A, s_u^A, the soil unit weight γ the excavation width B, excavation depth H_e, system stiffness $\ln(S)$, and wall penetration D on the base stability of braced excavations with consideration of anisotropy of the soil undrained shear strength. The influence of the parameters s_u^A, γ, s_u^P/s_u^A, and B/H_e are found to be more significant on the FS, compared with the parameters D/H_e, $\ln(S)$, and G_{ur}/s_u^A. A simple logarithmic regression (LR) model was developed for preliminary assessment of the basal heave factor of safety for braced excavations in anisotropic clay. The proposed estimation model was validated by 13 well-documented case histories from Hangzhou and Taiwan.

Fig. 15 Comparison of FS_S2 and FS_LR for case histories

Appendix: Python code for FEM batch calculation

```
Code for pre- and post-processing of the FEM in Python
from  openpyxl.reader.excel  import  load_workbook
from openpyxl import Workbook
import os,time,imp
import numpy as np
#Connect with PLAXISOutput
localhostport_output = 10001
plaxis_path = r'E:\Program Files\Plaxis\PLAXIS 2D'

from plxscripting.easy import *
localhostport_output=10001
s_o,g_o=new_server('localhost',localhostport_output,password='LLY2+G~4TsT@Z4s?')

path=r'H:\he=16_b_0.2'
modellist=[]
for i in os.listdir(path):
    if os.path.splitext(i)[1]==".p2dx":
        modellist.append(os.path.splitext(i)[0])

wb = Workbook()
ws = wb.active
ws.append(['Simulation #',  'Max. lateral wall deflection (10^-3 m)',
           'y[1]','strut force 1(kN*m/m)','y[2]','strut force 2 (kN*m/m)','y[3]',
'strut force 3 (kN*m/m)','y[4]','strut force 4 (kN*m/m)','FS', ])

ws.append([" "])

wb.save(str(path) + '/' + 'total.xlsx')

for i in range(0, len(modellist)):
    File_name=str(path)+'\\'+str(modellist[i])+'.p2dx'
    s_o.open(os.path.abspath(File_name))

    FS = g_o.echo(g_o.Phases[13].Reached.SumMsf)


    PlateUx = g_o.getresults(g_o.Phases[12], g_o.ResultTypes.Plate.Ux, 'node')
    strutY = g_o.getresults(g_o.Phases[12], g_o.ResultTypes.FixedEndAnchor.Y,
'node')
    strutN = g_o.getresults(g_o.Phases[12],
g_o.ResultTypes.FixedEndAnchor.AnchorForceMin2D, 'node')

    strutY = list(strutY)
    strutN = list(strutN)

    maxUx=min(PlateUx)
    Uxmax=round(maxUx*1000,3)

    wb = load_workbook(str(path) + '/' + 'total.xlsx')
    sheetnames = wb.get_sheet_names()
    ws = wb.get_sheet_by_name(sheetnames[0])
    ws.append([modellist[i], Uxmax, strutY[0], strutN[0], strutY[1], strutN[1],
strutY[2], strutN[2], strutY[3], strutN[3],FS, ])

    wb.save(str(path) + '/' + 'total.xlsx')

    s_o.close()
    time.sleep(0.5)

    print(str(path)+'/'+modellist[i]+"  is DONE")
    s_o.close()
```

References

1. Brinkgreve LBJ, Engin E, Swolfs WM (2017) Plaxis manual. PLAXIS bv, Netherlands
2. Bjerrum L, Eide O (1956) Stability of strutted excavations in clay. Geotechnique 6(1):32–47
3. Chowdhury SS (2017) Reliability analysis of excavation induced basal heave. Geotech Geol Eng 35(6):2705–2714
4. D'Ignazio M, Lansivaara T, Jostad HP (2017) Failure in anisotropic sensitive clays: a finite element study of the Pernio failure test. Can Geotech J 54:1013–1033
5. Freeman WS, Sutherland HB (1974) Slope stability analysis in anisotropic Winnipeg clays. Can Geotech J 11(1):59–71
6. Fu D, Zhang Y, Aamodt KK, Yan Y (2020) A multi-spring model for monopile analysis in soft clays. Mar Struct 72:102768
7. Grimstad G, Jostad HP, Andresen L (2010) Undrained capacity analyses of sensitive clays using the nonlocal strain approach. In: Proceedings of the 9th HSTAM international congress on mechanics, Vardoulakis mini-symposia, Limassol, Kypros, 12–14 July, pp 153–160
8. Grimstad G, Andresen L, Jostad HP (2012) NGI-ADP: Anisotropic shear strength model for clay. Int J Numer Anal Meth Geomech 36(4):483–497
9. Goh ATC (1990) Assessment of basal stability for braced excavation systems using the finite element method. Comput Geotech 10:325–338
10. Goh ATC, Kulhawy FH, Wong KS (2008) Reliability assessment of basal-heave stability for braced excavations in clay. J Geotech Geoenviron Eng 134(2):145–153
11. Goh ATC (2017) Basal heave stability of supported circular excavations in clay. Tunn Undergr Space Technol 61:145–149
12. Goh ATC, Zhang WG, Wong KS (2019) Deterministic and reliability analysis of basal heave stability for excavation in spatial variable soils. Comput Geotech 108:152–160
13. Hanson LA, Clough GW (1981) The significance of clay anisotropy in finite element analysis of supported excavations. In: Proceedings of symposium, implementation of computer procedure of stress strain laws in geotechnical engineering, vol I–II, Chicago, IL
14. Hsieh PG, Ou CY, Liu HT (2008) Basal heave analysis of excavations with consideration of anisotropic undrained strength of clay. Can Geotech J 45(6):788–799
15. Huang MS, Liu YH (2011) Simulation of yield characteristics and principal stress rotation effects of natural soft clay. Chin J Geotech Eng 33(11):1667–1675
16. Ismael M, Konietzky H, Herbst M (2019) A new continuum-based constitutive model for the simulation of the inherent anisotropy of Opalinus clay. Tunnel Undergr Space Technol 93:103106
17. Kung GTC, Hslao ECL, Schuster M, Juang CH (2007) A neural network approach to estimating deflection of diaphragm walls caused by excavation in clays. Comput Geotech 34(5):385–396. https://doi.org/10.1016/j.compgeo.2007.05.007
18. Kong DS, Men YQ, Wang LH, Zhang QH (2012) Basal heave stability analysis of deep foundation pits in anisotropic soft clays. J Central South Univ (Sci Technol) 43(11):4472–4476
19. Larsson R (1980) Undrained shear strength in stability calculation of embankments and foundations on soft clays. Can Geotech J 17(4):591–602
20. Larsson R, Sällfors G, Bengtsson P E, Alén C, Bergdahl U, Eriksson L (2007) Skjuvhällfasthet: utvärdering I kohesionsjord, 2nd edn. Information 3. Swedish Geotechnical Institute (SGI), Linköping
21. Li Y, Zhang W (2020) Investigation on passive pile responses subject to adjacent tunnelling in anisotropic clay. Comput Geotech. https://doi.org/10.1016/j.compgeo.2020.103782
22. Luo Z, Atamturktur S, Cai Y, Juang CH (2012) Reliability analysis of basal-heave in a braced excavation in a 2-D random field. Comput Geotech 39:27–37
23. Lyu HM, Shen SL, Wu YX, Zhou AN Calculation of groundwater head distribution with a close barrier during excavation dewatering in confined aquifer. Geosci Front 12(2):13
24. Shen Y (2007) Experimental study on effect of variation of principal stress orientation on undisturbed soft clay. Thesis, Zhejiang University, China
25. Skau KS, Chen Y, Jostad HP (2018) A numerical study of capacity and stiffness of circular skirted foundations in clay subjected to combined static and cyclic general loading. Géotechnique 68(3):205–220
26. Tang YG, Kung GTC (2011) Probabilistic analysis of basal heave in deep excavation. GeoRisk 2011: geotechnical risk assessment and management, Atlanta, 26-28 June 2011, pp 217–224. https://doi.org/10.1061/41183(418)13
27. Taiebat M, Kaynia AM, Dafalias YF (2011) Application of an anisotropic constitutive model for structured clay to seismic slope stability. J Geotech Geoenviron Eng 137(5):492–504
28. Terzaghi K (1943) Theoretical soil mechanics. Wiley, New York
29. Teng FC, Ou CY, Hsieh PG (2014) Measurements and numerical simulations of inherent stiffness anisotropy in soft Taipei clay. J Geotech Geoenviron Eng 140(1):237–250. https://doi.org/10.1061/(asce)gt.1943-5606.0001010
30. Ukritchon B, Boonyatee T (2015) Soil parameter optimization of the NGI-ADP constitutive model for bangkok soft clay. Geotech Eng 46(1):28–36
31. Wheeler SJ, Näätänen A, Karstunen M, Lojander M (2003) An anisotropic elasto-plastic model for soft clays. Can Geotech J 40(2):403–418
32. Wu SH, Ou CY, Ching JY, Juang CH (2012) Reliability-based design for basal heave stability of deep excavations in spatially varying soils. J Geotech Geoenviron Eng 138(5):594–603
33. Wu YX, Lyu HM, Han J, Shen SL (2019) Dewatering-induced building settlement around a deep excavation in soft deposit in Tianjin. China. J Geotech Geoenviron Eng 145(5):1–14
34. Wu YX, Shen SL, Yuan DJ (2016) Characteristics of dewatering induced drawdown curve under blocking effect of retaining wall in aquifer. J Hydrol 539:554–566
35. Ying HW, Zhang JH, Zhou J, Sun W, Yan JJ (2016) Analysis of stability against basal heave of excavation in anisotropic soft clay based on tests of hollow cylinder apparatus. Rock Soil Mech 37(5):1237–1248
36. Ying HW, Cheng K, Zhang LS, Ou CY, Yang YW (2020) Evaluation of excavation-induced movements through case histories in Hangzhou. Eng Comput 37(6):1993–2016
37. Yz A, Kha B (2019) Soil reaction curves for monopiles in clay. Mar Struct 65:94–113
38. Zdravkovic L, Potts DM, Hight DW (2002) The effect of strength anisotropy on the behaviour of embankments on soft ground. Geotechnique 52(6):447–457
39. Zhang WG, Goh ATC, Goh KH, Chew OYS, Zhou D, Zhang R (2018) Performance of braced excavation in residual soil with groundwater drawdown. Undergr Space 3:150–165

40. Zhang WG, Zhang RH, Wu CZ, Goh ATC, Lacasse S, Liu ZQ, Liu HL (2020) State-of-the-art review of soft computing applications in underground excavations. Geosci Front 11:1095–1106

41. Zhang RH, Wu CZ, Goh ATC, Thomas B, Zhang WG (2020) Estimation of diaphragm wall deflections for deep braced excavation in anisotropic clays using ensemble learning. Geosci Front. https://doi.org/10.1016/j.gsf.2020.03.003

42. Zhang WG, Zhang RH, Wu CZ, Goh ATC, Wang L (2020) Assessment of basal heave stability for braced excavations in anisotropic clay using extreme gradient boosting and random forest regression. Undergr Space. https://doi.org/10.1016/j.undsp.2020.03.001